

Rheological Behavior of Microemulsions

G. Gonnella and M. Ruggieri

Istituto Nazionale per la Fisica della Materia, Unità di Bari and Dipartimento di Fisica, Università di Bari, and Istituto Nazionale di Fisica Nucleare, Sezione di Bari, via Amendola 173, 70126 Bari, Italy.

(October 30, 2018)

We study the stationary and transient behaviors of the microemulsion phase subjected to a shear flow. The system is described by a diffusion-convective equation which generalizes the usual Cahn-Hilliard equation. Non-linear terms are treated in a self-consistent approximation. Shear, first and second normal stresses are calculated as momenta of the structure factor. Shear thinning is observed in stationary conditions. After a newtonian regime at small values of the shear rate, the excess viscosity decreases when the shear rate becomes of the order of the inverse of the relaxation time of the system without flow. In transient regimes, when the flow is applied starting from a quiescent state, we find that the shear stress reaches a maximum before decreasing to a constant value.

61.20.Gy; 82.70.-y; 83.50.Ax

I. INTRODUCTION

The rheological behavior of complex fluids such as polymer solutions, polymer melts, emulsions is of considerable interest both in technology and in basic research [1]. While the behavior of the stress response to applied flows is of fundamental importance in many applications, it also reflects the existence of mesoscopic structures in the fluid and is intimately related to its constitution. For example, when a shear flow is applied to a polymer solution, the stress first reaches a maximum and then relaxes to a constant value [2]. This phenomenon, at small strain, is related to the entanglement of the polymer network which is distorted by the flow with a resulting increase of the stress. At larger values of the strain, however, the disentanglement of the system is favoured and the stress is observed to decrease. In general, non monotonic relaxational properties of the stress are typical of complex fluids which are also characterized, in stationary conditions, by non-newtonian behavior. The effective viscosity depends on the applied shear flow and different behaviors can be observed [1].

In this paper we consider the rheological behavior of the microemulsion phase both in stationary and transient conditions. In ternary self-assembling systems the surfactant forms interfaces between oil- and water-like domains. These interfaces, in the microemulsion phase, constitute an intertwined bicontinuous structure disordered on large scales but with mesoscopic order on distances of the order of 500 Angstroms [3]. The observed structure factor is given by

$$I(q) \sim \frac{1}{a + gq^2 + cq^4} \quad (1)$$

which, for $g < 0$, has a maximum at $q = \sqrt{\frac{|g|}{2c}}$ [4-6]. In real space, this corresponds to the two-point correlation function

$$G(r) = \frac{d}{2\pi r} e^{-r/\xi} \sin\left(\frac{2\pi r}{d}\right) \quad (2)$$

where ξ plays the role of the usual correlation length in disordered phases, d is related to the size of coherent regions of oil or water domains, and typical values of the ratio d/ξ are in the interval 2 – 4.

The behavior of the stress in the microemulsion phase was first considered in [7] and then in [8] where also the two-time correlation functions were studied. Here we complete the analysis of the steady state of [8] and consider also the transient behavior. Our approach is based on the use of a continuum free-energy functional and is similar to that of Onuki and Kawasaki [9], applied also to evaluate the effects of a shear flow on copolymer melts [10,11], on the disorder-lamellar transition [13,14], and on the phase separation of binary mixtures [15].

We consider a Cahn-Hilliard equation generalized by the presence of a convective term. Hydrodynamical effects are neglected; moreover, the surfactant is assumed to relax faster than the other components of the mixture so that its degrees of freedom are not explicitly considered. Non-linear terms, which become relevant close to transition lines, will be treated self-consistently. A renormalization procedure is introduced and the system is studied in terms of the physical variables ξ, d of the case without flow.

Our main result for the stationary regime is the behavior of the constitutive curve. Shear thinning, which is the decreasing of the effective viscosity when the shear rate is increased, is observed in two different ranges of the shear rate. It first occurs at a value of the shear rate of the order of the inverse of the relaxation time of microemulsions without shear. The morphological changes occurring when the shear rate is increased can be deduced by the patterns exhibited by the structure factor. In the transient behavior after the application of the flow, at sufficiently high shear rates, we observe a maximum in the shear stress followed by a relaxation to a constant value, analogously to what observed in other systems. We have also studied the behavior of the stress tensor when, starting from a stationary state with shear, the flow is switched off.

The paper is divided as follows. In Section 2 we specify the model and solve formally the dynamical equation for the structure factor. Results for the stationary regime and for the transients are respectively described in Sections 3 and 4. Section 5 contains some conclusions.

II. THE MODEL

Our study of rheological properties of microemulsions is based on a functional Landau-Ginzburg approach with one scalar order parameter $\phi(\vec{x})$ representing the concentration difference between oil and water. We consider the hamiltonian

$$\mathcal{H}[\phi] = \int d^3x \left\{ \frac{1}{2} \left[a_2 \phi^2 + (g_0 + g_2 \phi^2) (\vec{\nabla} \phi)^2 + c (\nabla^2 \phi)^2 \right] + \frac{\lambda}{4} \phi^4 \right\} \quad (3)$$

which has been largely demonstrated to well describe equilibrium properties of ternary mixtures [3]. Here we briefly discuss the properties of this hamiltonian relevant for the microemulsion phase. The expression (3) differs in the gradient terms from the usual Landau-Ginzburg hamiltonian used to study binary mixtures. A negative value of the function $g(\phi) = g_0 + g_2 \phi^2$ ($g_2 > 0$) favors the appearing of interfaces. In particular the value of g_0 can be related to the amount of surfactant present in the system. The term proportional to $c > 0$ assures stability at large momenta and weights the curvature of interfaces.

The presence of the quartic terms ϕ^4 and $\phi^2 (\vec{\nabla} \phi)^2$, which also in a disordered phase could have a role in the proximity of a transition line, makes impossible an exact determination of the two point correlation functions. However, following [7], it is possible to use a renormalization procedure based on a self-consistent approximation to find an expression for the equilibrium scattering function and for the two-point correlation function in real space. For the first, defined $\phi(\vec{k})$ the Fourier transform of $\phi(\vec{x})$, it is found that

$$S(k) \equiv \langle \phi(\vec{k}) \phi(-\vec{k}) \rangle = \frac{T}{a_r + g_r k^2 + c k^4} \quad (4)$$

where $k \equiv |\vec{k}|$, the renormalized parameters are given by

$$a_r = a_2 + \lambda \mathcal{S}_0 + g_2 \mathcal{S}_2 \quad (5)$$

$$g_r = g_0 + g_2 \mathcal{S}_0 \quad (6)$$

and the loop integrals are defined as

$$\mathcal{S}_p = \int_{|\vec{k}| < \Lambda} \frac{d^3 \vec{k}}{(2\pi)^3} k^p S(k) \quad (7)$$

($p = 0, 2$) with Λ being a high momentum phenomenological cut-off. The region $g_r < 0$ and $4a_r c - g_r^2 > 0$,

as discussed in the introduction, can be identified with the microemulsion phase with the function $S(k)$ having a peak at $k \equiv k_M = \sqrt{\frac{|g_r|}{2c}}$. Moreover, the characteristic lengths ξ and d appearing in the real space two-point correlation function (2) are given by

$$\xi = \left[\frac{1}{2} \left(\frac{a_r}{c} \right)^{1/2} + \frac{1}{4} \left(\frac{g_r}{c} \right) \right]^{\frac{1}{2}} \quad (8)$$

$$d = 2\pi \left[\frac{1}{2} \left(\frac{a_r}{c} \right)^{1/2} - \frac{1}{4} \left(\frac{g_r}{c} \right) \right]^{\frac{1}{2}} \quad (9)$$

Therefore equilibrium properties can be expressed in terms of renormalized parameters and, by equations (8) and (9), through the physical lengths ξ and d (once the parameters λ , c , g_2 and the cut-off Λ are given).

The dynamics of the order parameter in presence of convective motion [16] is described by the equation:

$$\frac{\partial \phi}{\partial t} + \vec{v} \cdot \vec{\nabla} \phi = \Gamma \nabla^2 \left(\frac{\delta \mathcal{H}}{\delta \phi} \right) + \eta_\phi \quad (10)$$

where \mathcal{H} is the hamiltonian of (3). The velocity field \vec{v} is a planar Couette shear flow:

$$\vec{v} = \gamma y \vec{e}_x \quad (11)$$

where γ is the shear rate and \vec{e}_x the unit vector in the flow direction; η_ϕ is a white gaussian noise representing thermal fluctuations with momenta given by

$$\langle \eta_\phi(\vec{x}, t) \rangle = 0 \quad (12)$$

$$\langle \eta_\phi(\vec{x}, t) \eta_\phi(\vec{x}', t') \rangle = -2T \Gamma \nabla^2 \delta^3(\vec{x} - \vec{x}') \delta(t - t') \quad (13)$$

($\langle \dots \rangle$ means the ensemble average) as required by the Fluctuation-Dissipation theorem which holds in absence of flow. The functional derivative $\delta \mathcal{H} / \delta \phi$ represents the difference in chemical potentials between oil and water; Γ is a mobility coefficient and T is the temperature of the heat bath. By assuming equation (10) as the evolution equation for ϕ , we are neglecting hydrodynamics fluctuations as well as the motion of the surfactant.

We will study the evolution equation for the dynamical structure factor

$$S(\vec{k}, t) \equiv \langle \phi(\vec{k}, t) \phi(-\vec{k}, t) \rangle \quad (14)$$

in the same self-consistent approximation used in equilibrium to write Eqs. (5,6). The convection-diffusion equation can be formally linearized as [17]

$$\frac{\partial \phi}{\partial t} + \vec{v} \cdot \vec{\nabla} \phi = \Gamma \nabla^2 \{ (a_2 + \lambda \mathcal{S}_0(t) + g_2 \mathcal{S}_2(t)) \phi - (g_0 + g_2 \mathcal{S}_0(t)) \nabla^2 \phi + c \Delta^2 \phi \} + \eta_\phi \quad (15)$$

where the quantities $\mathcal{S}_p(t)$ are given by expressions analogue to those of Eq. (7) but now with $S(\vec{k}, t)$ of Eq. (14) self-consistently calculated with Eq. (15). A standard

procedure gives from Eq. (15) the dynamical equation for $S(\vec{k}, t)$:

$$\left\{ \frac{\partial}{\partial t} - \gamma k_x \frac{\partial}{\partial k_y} + 2\Gamma k^2 K_R(k) \right\} S(\vec{k}, t) = 2T\Gamma k^2 \quad (16)$$

where $K_R(k) \equiv a_r + g_r k^2 + ck^4$ is the renormalized vertex function and the parameters a_r and g_r can be obtained as in Eqs. (5,6) using $\mathcal{S}_p(t)$.

A formal solution of Eq. (16) may be obtained by the method of characteristics:

$$S(\vec{k}, t) = \Delta_0(\vec{K}(t)) \mathcal{I}_1(t) + 2T\Gamma \mathcal{I}_2(t) \quad (17)$$

where we have defined the functions

$$\mathcal{I}_1(t) = e^{-2\Gamma \int_0^t ds \mathcal{K}^2(s)[a_r + g_r \mathcal{K}^2(s) + c\mathcal{K}^4(s)]} \quad (18)$$

$$\mathcal{I}_2(t) = \int_0^t du \mathcal{K}^2(u) \mathcal{I}_1(u) \quad (19)$$

and $\vec{K}(u) \equiv \vec{k} + \gamma k_x u \vec{e}_y$; $\Delta_0(\vec{k})$ is the structure factor at the initial time $t = 0$. Since the quantities a_r and g_r contains the momenta of $S(\vec{k}, t)$, Equation (17) is actually a nonlinear integral equation for $S(\vec{k}, t)$. This equation can be solved numerically at each time by iterative methods.

Our results will first concern steady state properties. The stationary solution can be readily obtained from the $t \rightarrow +\infty$ limit of Eq. (17), observing that in this limit the first term of the solution tends to zero (except for the $\vec{k} = 0$ mode). Therefore we write the stationary structure factor as:

$$S(\vec{k}; \gamma)_\infty = 2T\Gamma \mathcal{I}_2(\infty) \quad (20)$$

where

$$\mathcal{I}_2(\infty) = \int_0^\infty dz \mathcal{K}^2(z) e^{-2\Gamma \int_0^z ds \mathcal{K}^2(s)[a_r + g_r \mathcal{K}^2(s) + c\mathcal{K}^4(s)]}$$

We will also study transient behaviors with the fluid evolving from a quiescent state towards the stationary state with shear, or with the system relaxing, after interruption of the flow, from the sheared stationary state into the quiescent state. For the latter case we use the solution of equation (16) with $\gamma = 0$:

$$S(\vec{k}; \gamma; t)_{relax} = S(\vec{k}; \gamma)_\infty e^{-2\Gamma k^2 K_R(k)} + \frac{T}{K_R(k)} \left(1 - e^{-\frac{t}{2\Gamma k^2 K_R(k)}} \right) \quad (21)$$

Finally, once the structure factor is known, we may evaluate the stresses which can be obtained as momenta of the structure factor [7]. The shear, first and second normal stresses are respectively given by

$$\sigma_{xy}(t) = - \int_{|\vec{k}| < \Lambda} \frac{d^3 \vec{k}}{(2\pi)^3} k_x k_y (g_r + 2ck^2) S(\vec{k}, t) \quad (22)$$

$$N_1(t) = - \int_{|\vec{k}| < \Lambda} \frac{d^3 \vec{k}}{(2\pi)^3} (k_x^2 - k_y^2) (g_r + 2ck^2) S(\vec{k}, t) \quad (23)$$

$$N_2(t) = - \int_{|\vec{k}| < \Lambda} \frac{d^3 \vec{k}}{(2\pi)^3} (k_y^2 - k_z^2) (g_r + 2ck^2) S(\vec{k}, t) \quad (24)$$

In addition, the excess viscosity is defined as:

$$\Delta\eta(t) = \frac{\sigma_{xy}}{\gamma} \quad (25)$$

which represents the contribution of interfaces to the full viscosity of the fluid (that is, evaluating the viscosity of the fluid by means of equation (25) we are neglecting the hydrodynamical contribution to the viscosity itself).

III. STATIONARY REGIME

In this section we present results for the steady states reached under the action of the shear flow with the structure factor given by Eq. (20). We have studied numerically this expression for several values of ξ, d and γ . The other parameters have been fixed as $g_2 = 1, c = 1, \lambda = 0.5, \Lambda = 3$.

The effects of the flow on the structure factor can be seen in Fig. 1 where the projections on the planes $k_y = 0$ and $k_z = 0$ are shown for different γ and $\xi = 2, d = 6$. Similar results have been obtained for other choices of ξ and d [8]. (At $k_x = 0$ the shape of the structure factor is the same of the case without flow, see Eq. (16)). At $\gamma = 0.5$ the structure factor remains almost isotropic and its pattern for each cartesian plane is close to that of a circular volcano. The patterns are progressively distorted when the shear rate is increased. On the plane $k_z = 0$, at $\gamma = 2$, the edge of the volcano has assumed an elliptical shape and four peaks are visible. These peaks initially appear on the coordinate axes; then, when γ is increased, the ones located at $k_x \simeq 0$ become comparatively more important while the two others rotate clockwise and decrease their amplitude linearly with γ until they disappear. Indeed, in the limit $\gamma \rightarrow \infty$, since terms proportional to powers of γk_x damp the exponential term on the r.h.s. of Eq. (20), only the maxima of $C(\vec{k})$ with $k_x = 0$ and $k_y = \pm k_M$ survive. On the other plane $k_y = 0$ two peaks at $k_x = 0, k_z = \pm k_M$, are also observed to become sharper and sharper as γ is increased.

The above results can be related to the orientation of the interfaces in the mixture, as also observed in [8]. A peak of $C(k)$ defines a characteristic length proportional to the inverse of its position and, since the system is not isotropic, to each maximum one associates three lengths, one for each space direction. Due to the symmetry $\vec{k} \rightarrow -\vec{k}$ only the peaks not related by reflection around the origin can be considered. At very large shear rate the existence of a single couple of maxima at $k_x = 0$ signals that interfaces are preferentially aligned along the flow with symmetry recovered in the transverse directions and the characteristic lengths being the same as without shear. For intermediate values of γ the additional peaks at $(\tilde{k}_x, \tilde{k}_y, \tilde{k}_z)$ reveal the presence of interfaces oriented with an angle $\alpha = \arctan(-\tilde{k}_x/\tilde{k}_y)$ with respect to the flow, besides those aligned along the x direction. These additional peaks are better seen in a region of parameters

closer to the microemulsion-lamellar transition line corresponding to a larger value of ξ [8]. As γ is increased the tilt angle α and the relative abundance of lamellae oriented at this angle diminish as suggested by the behavior of the maxima with $k_x \neq 0$ previously discussed.

The behavior of the stress tensor as a function of the shear rate is reported in Figs. 2-4. At small values of γ the shear stress is a linear function of γ so that the viscosity is constant and the fluid is newtonian. Shear thinning occurs for γ between 1 and 2, when the slope of the curve of the stress changes significantly. At this point the original volcano shape of the structure factor has also appreciably changed. In terms of interfaces we expect that, when shear thinning is observed, the bicontinuous network of interfaces which is only distorted in the newtonian regime, is affected by many ruptures with a significant decrease of connectivity. We can say that a strong shear regime is entered. Indeed, we can compare the shear temporal scale γ^{-1} with the relaxation time τ_M of microemulsions in equilibrium. The relaxation time of a mode with wavevector k is given by

$$\tau(\vec{k}) = \frac{1}{\Gamma k^2 (a_r + g_r k^2 + c k^4)} \quad (26)$$

Following [7] we choose $k = k_M$ corresponding to the peak of microemulsions, so that

$$\tau_M = \frac{1}{8\Gamma c} \frac{\xi^2 d^2}{4\pi^2 [(2\pi^2/d)^2 - 1/\xi^2]} \quad (27)$$

The corresponding Deborah number is given by

$$De = \frac{\tau_M}{\tau_S} \quad (28)$$

where $\tau_S = 1/\gamma$. If we take $\gamma = 2$ we get $De \sim 1.9$ for the case of Fig. 2. This indicates that shear thinning becomes evident when the shear rate is of the order of the inverse of typical structural times of the system without shear. We checked for other values of ξ, d that the Deborah number at shear thinning is always of order 1.

Shear thinning is observed again at $\gamma \sim 10^3$ when, as we have seen, peaks with $k_x = 0$ largely prevail. We expect that at these values of the shear rate the original bicontinuous interface network has changed significantly its topology becoming more similar to a stack of lamellae. At very large γ the excess viscosity is found to decrease as $1/\gamma^{-s}$ with $s = 1.87$ which is close to the analytical limit $s = 2$ [7]. In this final stress regime the lamellae are expected to become more and more aligned with the flow with fluctuations very inhibited. We observe that the shear stress corresponding to a completely ordered lamellar phase is zero.

The other stress components N_1, N_2 behave similarly. At small γ , $N_1, N_2 \sim \gamma^2$ while they decrease as γ^{-1} when $\gamma \rightarrow \infty$ (see Figs. 3-4).

IV. TRANSIENTS

We have studied the evolution of the system under the action of the shear flow from the initial equilibrium configuration of Eq.(4) towards the steady state of the previous section, as described by Eq. (17). The behavior of the stress components for different values of γ is shown in Figs. 5-7. When γ is large enough that $De \geq 1$, a non monotonic behavior of the stress is observed with $\sigma_{xy}, N_1, |N_2|$ exhibiting a maximum before relaxing to a constant value. A similar behavior has been measured in polymer solutions [2]. In our case we can think that at initial times the surfactant interfaces are stretched by the flow with a consequent increase of the stress. When the maximum of the stress is reached, the interface structure starts to be broken and the stress relaxes to a lower value. The temporal evolution of the structure factor for $\gamma = 100$ is shown in Fig. 8. The largest observed distortion corresponds to the maximum of the stress. In the case $\gamma = 2$, when the relaxation of the stress is monotonic, a prolate pattern like that in the middle of Fig.8 at $k_z = 0$ is not observed.

We have also considered the opposite situation with the system, initially in a stationary state with shear, evolving without flow as described by Eq. (21). In this case the behavior is exponentially monotonic after an initial faster decay, as it can be seen in Fig. 9. The time constant τ of the exponential part of the relaxation decreases with γ , as shown in Fig. 10.

V. CONCLUSIONS

We have used a generalized Cahn-Hilliard equation with a convective term to study the rheological behavior of the microemulsion phase. The steady state constitutive curve shows shear thinning first occurring at a shear rate of the order of the inverse of the equilibrium relaxation time. We have also obtained for the first time analytical expressions for the temporal behavior of the structure factor. From this we derive a non monotonic evolution of the stress. This is similar to what is observed in other systems that relax into the steady state with a shear flow. We hope that these predictions are useful for future experiments. From the theoretical point of view this analysis can be completed studying how the equilibrium phase diagram, including the disorder and the Lifshitz lines [3-6], is changed by the presence of the flow. Moreover, hydrodynamic fluctuations should be taken into account for a full description of the system.

ACKNOWLEDGMENTS

We thank Antonio Lamura and Federico Corberi for helpful discussions. G.G acknowledges support by PRA-

- [1] See, e.g., R.G. Larson, *The structure and Rheology of Complex fluids* (34 Oxford University Press, New York, 1999).
- [2] Z. Laufer, H.L. Jalink, and A.J. Staverman, *Journal of Polymer Science* **11**, 3005 (1973).
- [3] For a review see, e.g., G. Gompper and M. Schick, *Self-assembling amphiphilic systems in Phase Transitions and Critical Phenomena*, edited by C. Domb and J.L. Lebowitz (Academic Press, New York, 1994), vol.16; K.A. Dawson in *Structure and Dynamics of Strongly Interacting Colloids and Supramolecular Aggregates in Solution*, edited by S.-H.Chen et al. (Kluwer Academic Publ. 1992).
- [4] M. Teubner and R. Strey, *J. Chem. Phys.* **87**, 3195 (1987).
- [5] B. Widom, *J. Chem. Phys.* **90**, 2437 (1989).
- [6] A. Cappi, P. Colangelo, G. Gonnella, and A. Maritan, *Nucl. Phys. B* **370**, 659 (1992); P. Colangelo, G. Gonnella, and A. Maritan, *Phys. Rev. E* **47**, 411 (1993); G. Gonnella and J.M.J. van Leuween, *Phys. Rev. E*, **52**, 63 (1995).
- [7] G. Pätzold and K. Dawson, *Phys. Rev. E* **54**, 1669 (1996); G. Pätzold and K. Dawson, *J. Chem. Phys.* **104**, 5932 (1996).
- [8] F. Corberi, G. Gonnella, and D. Suppa, *Phys. Rev. E* **63**, 040501(R).
- [9] A. Onuki and K. Kawasaki, *Ann. Phys. (N.Y.)* **121**, 456 (1979).
- [10] G.H. Fredrickson, *J. Chem. Phys.* **85**, 5306 (1986).
- [11] G.H. Fredrickson and R.G. Larson, *J. Chem. Phys.* **86**, 1553 (1987).
- [12] A. Onuki, *J. Chem. Phys.* **87**, 3692 (1987).
- [13] M.E. Cates and S.T. Milner, *Phys. Rev. Lett.* **62**, 1856 (1989).
- [14] C. Huang and M. Muthukumar, *J. Chem. Phys.* **107**, 5561 (1997).
- [15] F. Corberi, G. Gonnella, and A. Lamura, *Phys. Rev. Lett.* **81**, 3852 (1998); *Phys. Rev. Lett.* **83**, 4057 (1999);
- [16] A. Onuki, *J. Phys.: Condens. Matter* **9**, 6119 (1997).
- [17] The approximation corresponds to take the limit $N \rightarrow \infty$ in a model where the field ϕ is generalized to have N components. This approximation differs only by a factor $1/3$ multiplying λ from the one-loop calculation of [7] and, for the purposes of this paper, is equivalent to the one-loop approximation.

FIGURES

FIG. 1. Projections of the structure factor in the stationary state on the planes $k_y = 0$ (right column) and $k_z = 0$ (left column) for $\xi = 2$, $d = 6$. The shear rate is, from the top to the bottom, $\gamma = 0.5$, $\gamma = 2$, and $\gamma = 100$; k_x, k_y, k_z vary between -3 and 3 in adimensional units.

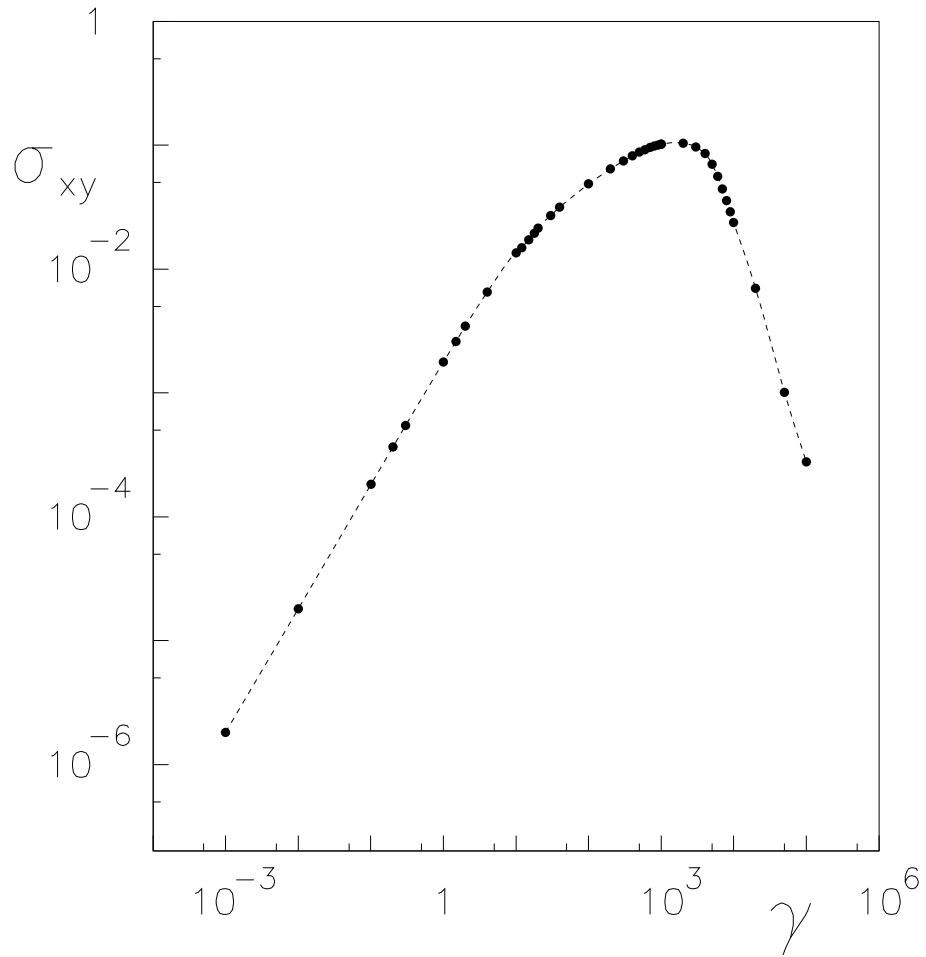


FIG. 2. The stationary shear stress σ_{xy} versus the shear rate γ for $\xi = 2$ and $d = 6$.

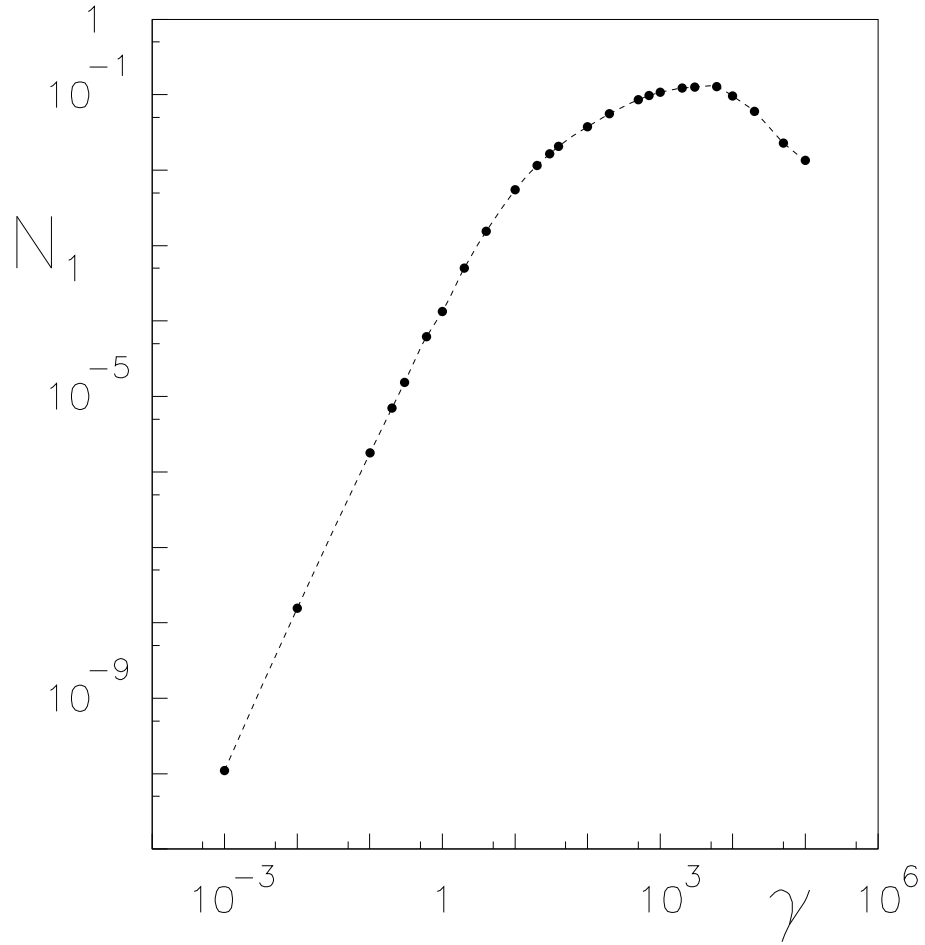


FIG. 3. The first normal stress N_1 for $\xi = 2$ and $d = 6$.

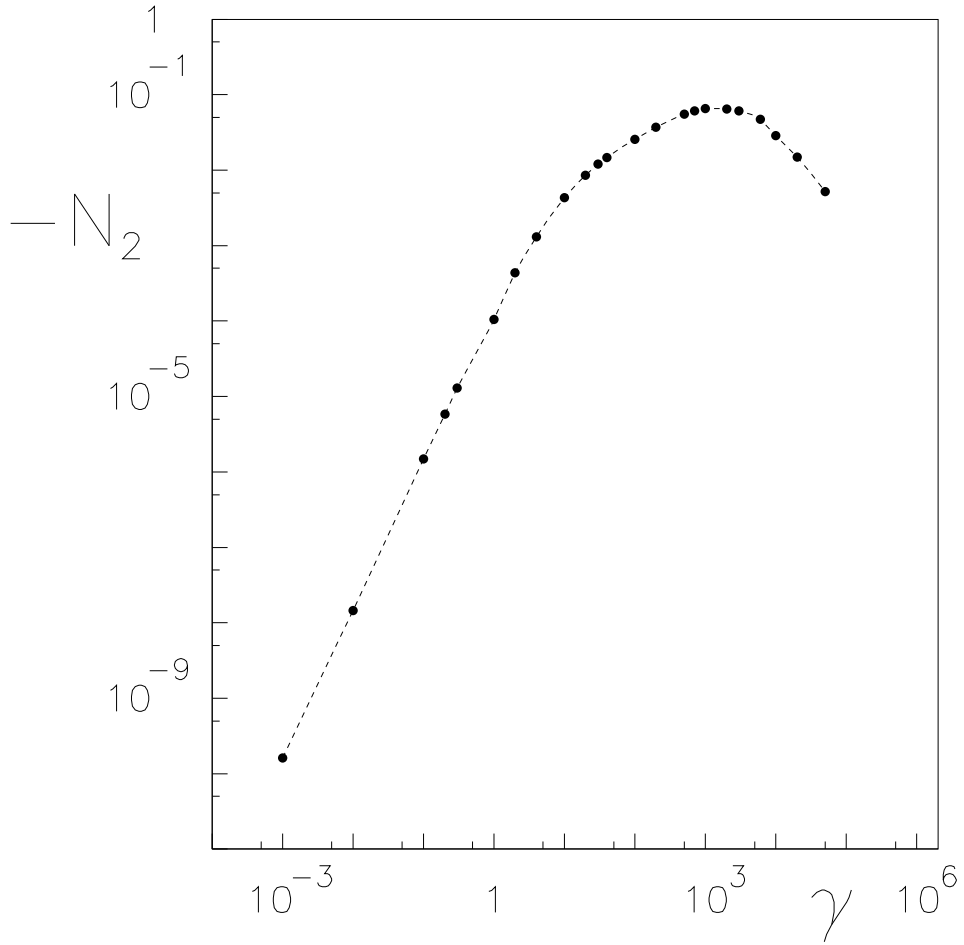


FIG. 4. Absolute value of the second normal stress N_2 for $\xi = 2$ and $d = 6$.

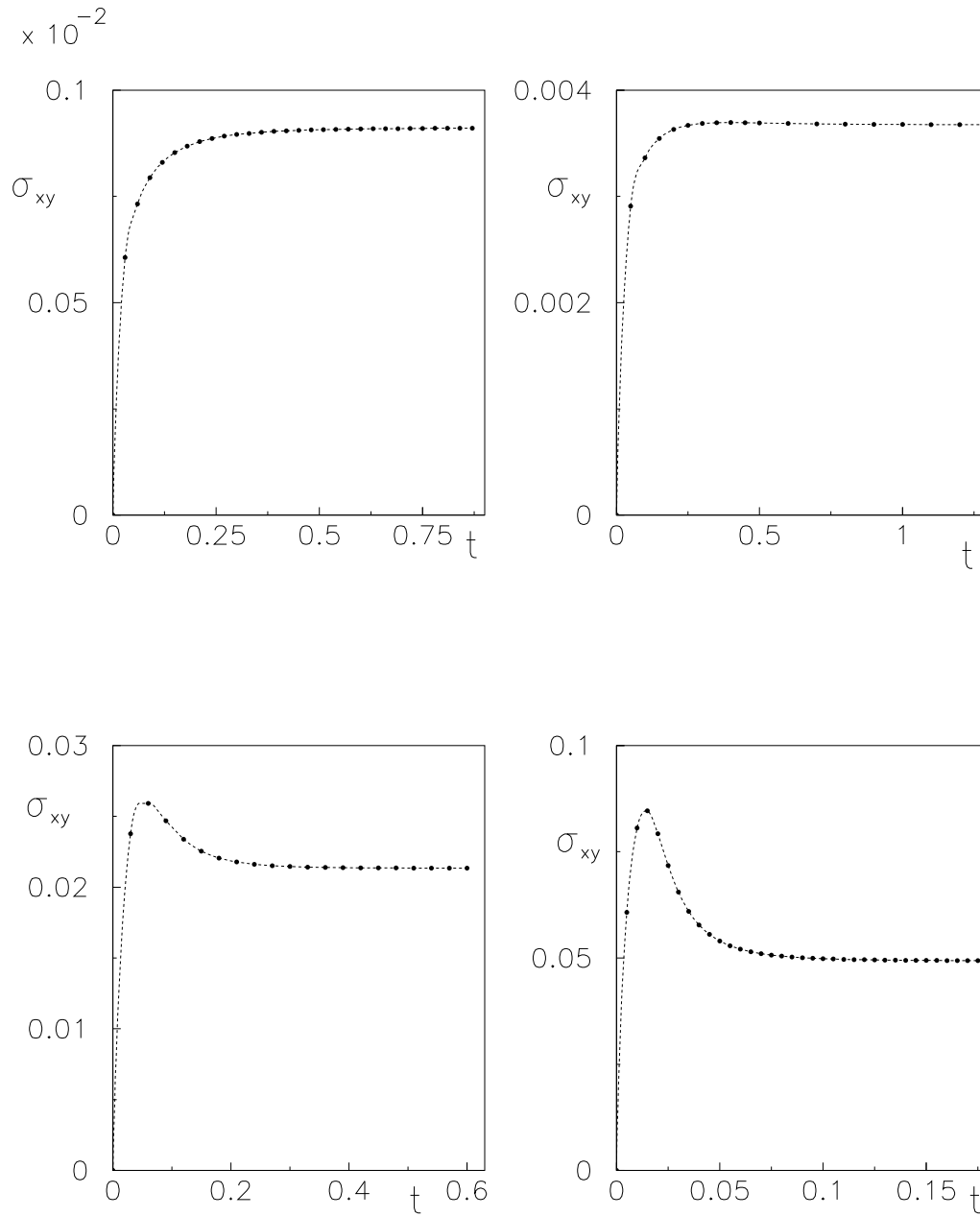


FIG. 5. Time evolution of the stress σ_{xy} for various values of the shear rate γ with $\xi = 2$ and $d = 6$. Results are shown for $\gamma = 0.5$ (top-left), $\gamma = 2$ (top-right), $\gamma = 20$ (bottom-left) and $\gamma = 100$ (bottom-right).

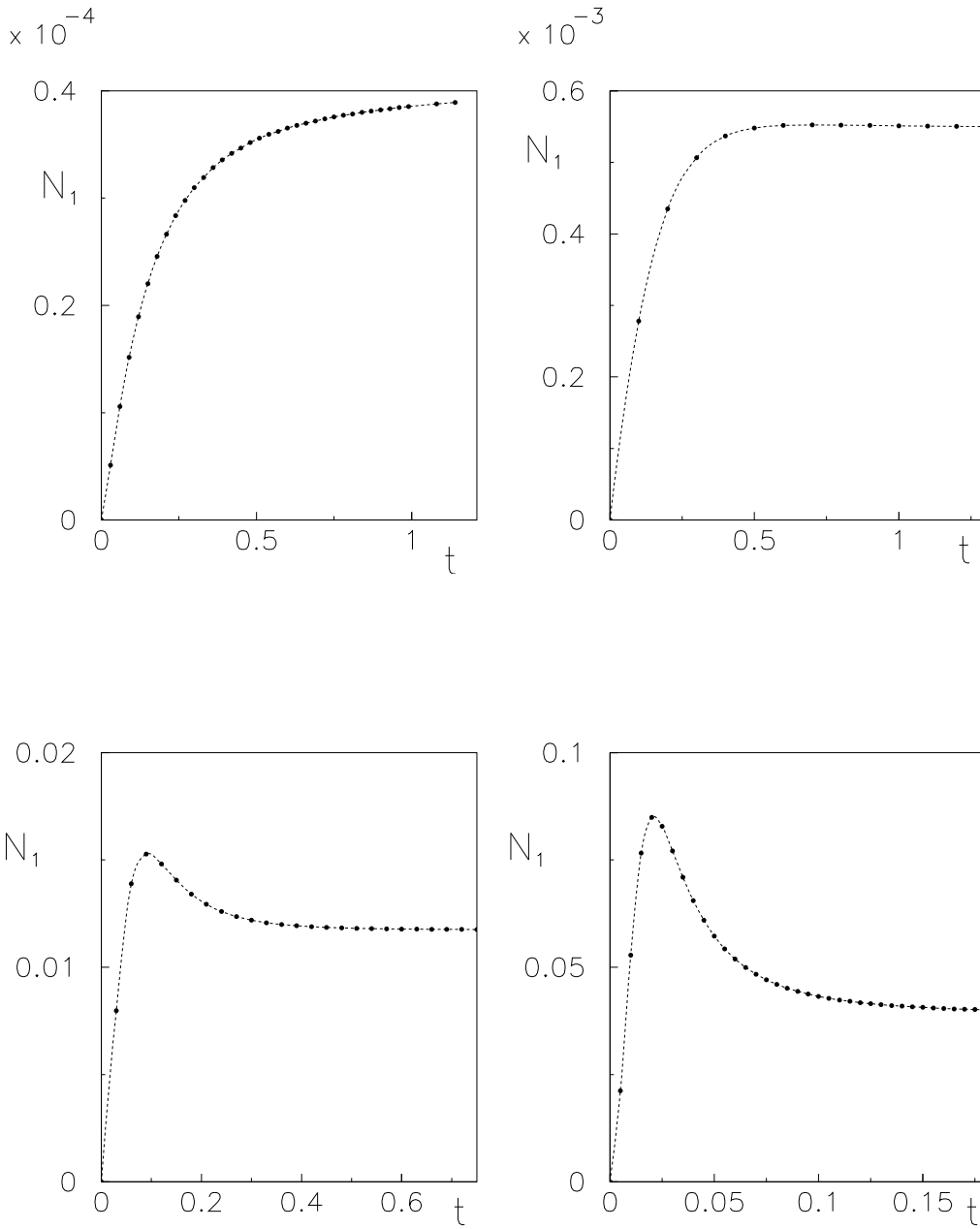


FIG. 6. Time evolution of the first normal stress N_1 ; the parameters are the same of Fig.5.

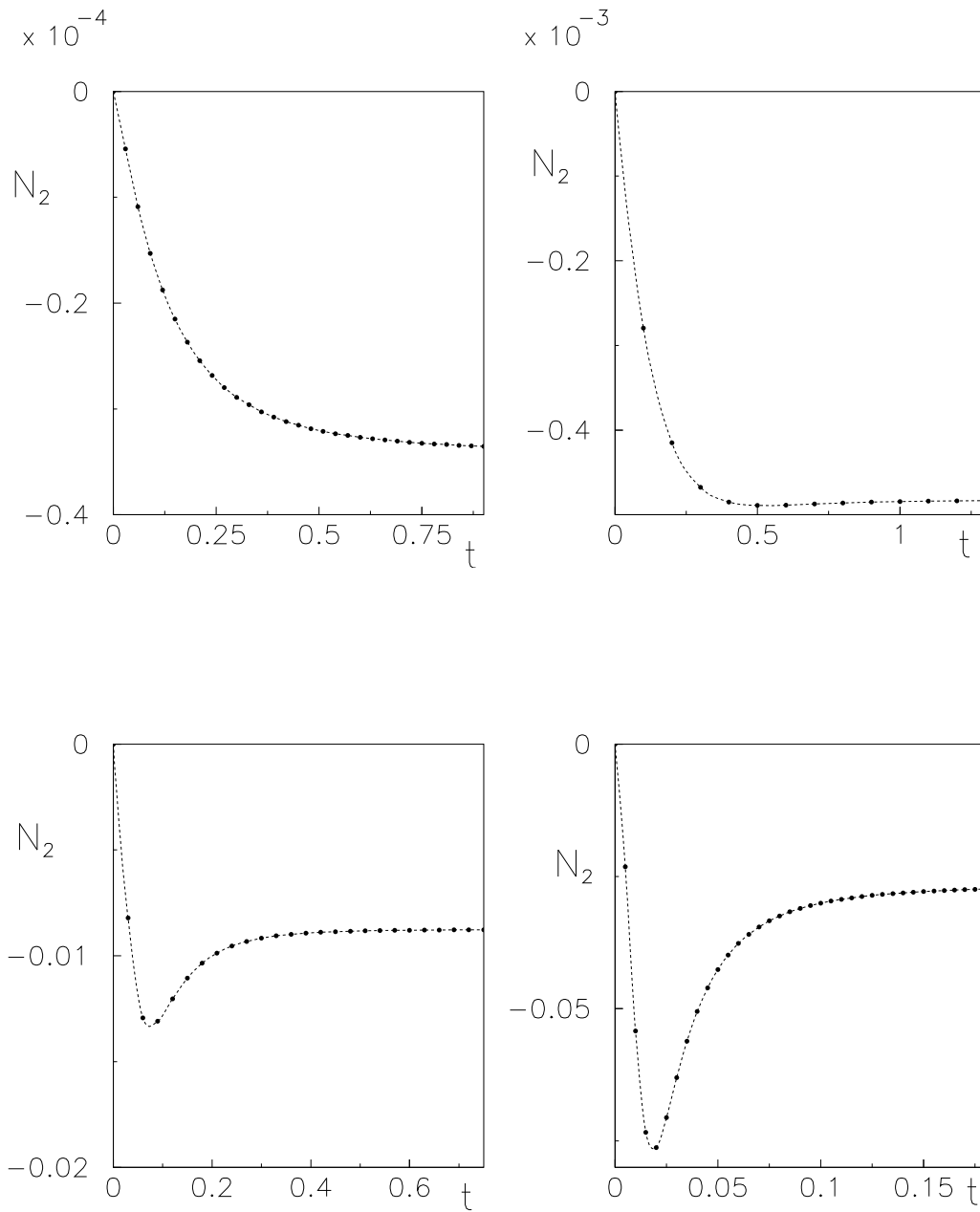


FIG. 7. Time evolution of the second normal stress N_2 with parameters as in Fig.5.

FIG. 8. Time evolution of the structure factor for $\xi = 2$, $d = 6$, and $\gamma = 100$. The projections on the planes $k_z = 0$ (left column) and $k_y = 0$ (right column) are shown respectively for $t = 0$ (top), $t = 2.5 \times 10^{-2}$ (middle), when the maximum of σ_{xy} is reached, and $t = 2.0 \times 10^{-1}$ (bottom).

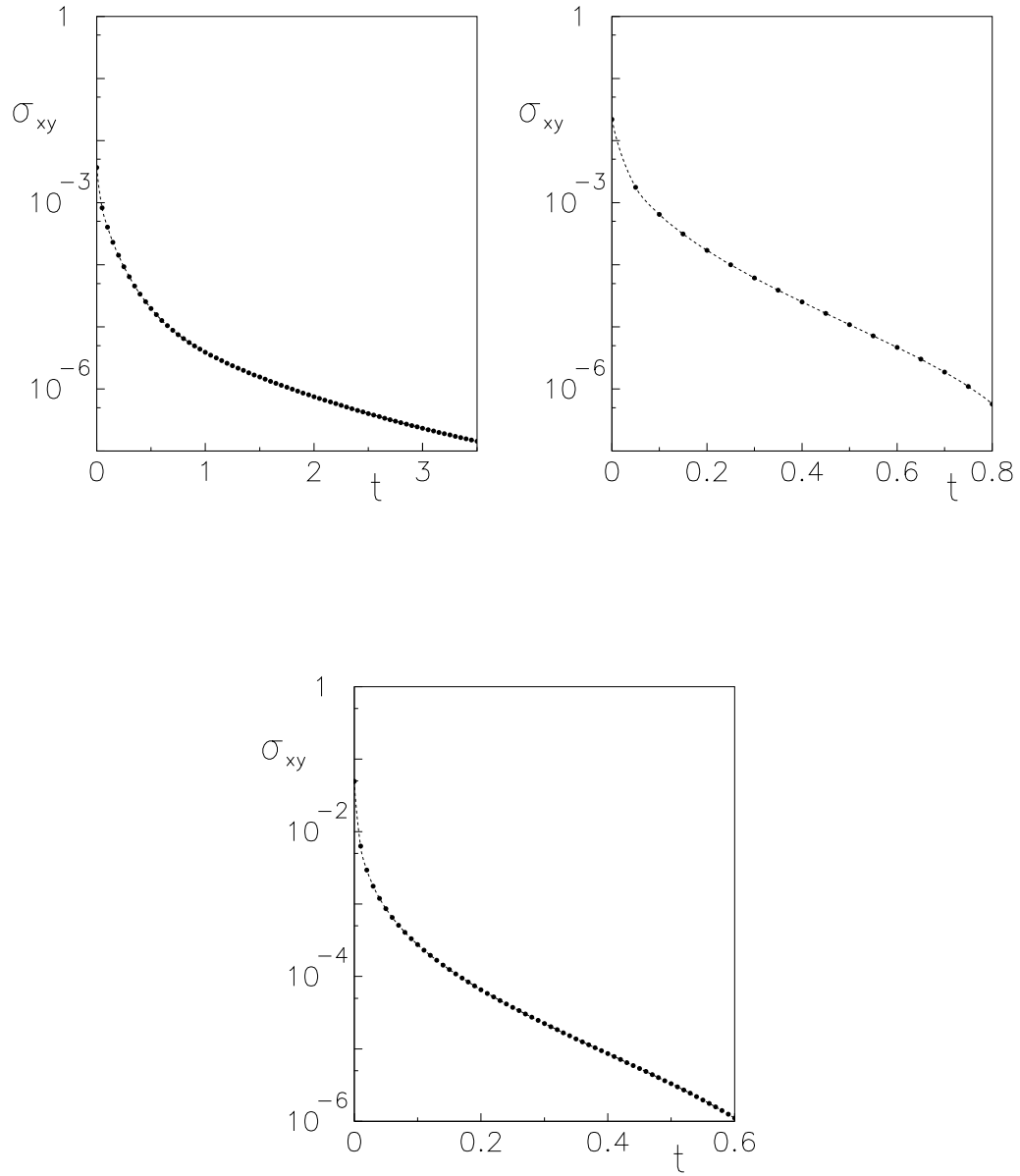


FIG. 9. Relaxation of the stress σ_{xy} for $\xi = 2$, $d = 6$, $\gamma = 2$ (top-left), $\gamma = 20$ (top-right) and $\gamma = 100$ (bottom).

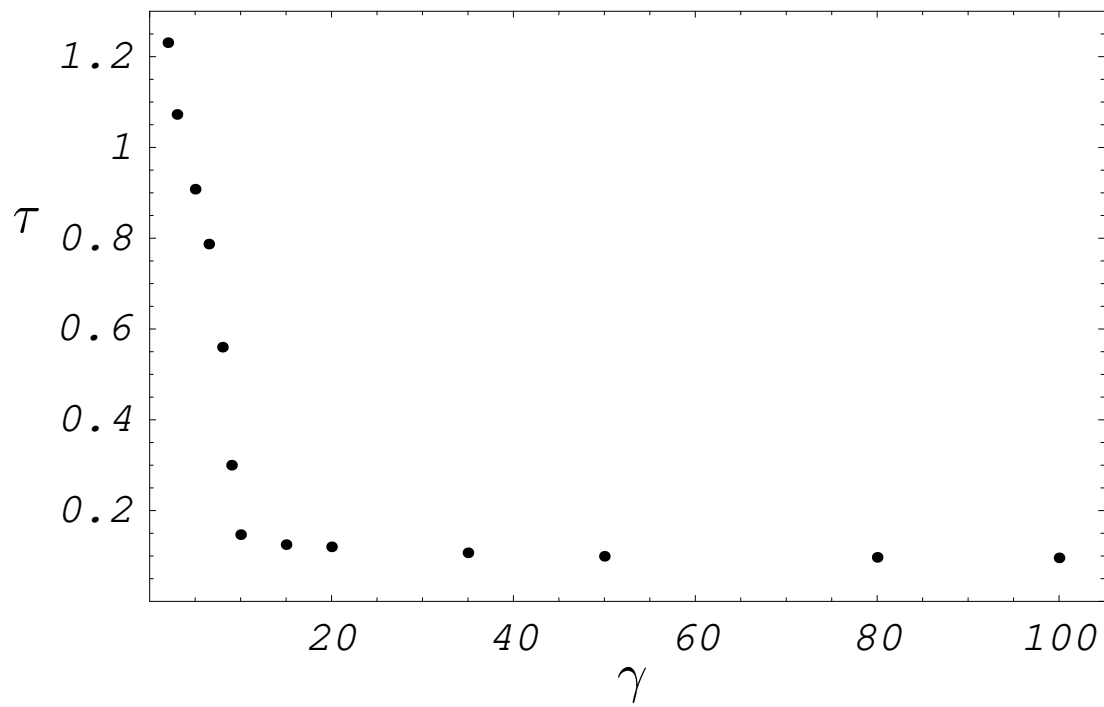


FIG. 10. Relaxation time τ as a function of the shear rate γ .

This figure "ruggfig1.jpg" is available in "jpg" format from:

<http://arxiv.org/ps/cond-mat/0210300v1>

This figure "ruggfig8.jpg" is available in "jpg" format from:

<http://arxiv.org/ps/cond-mat/0210300v1>